A New Concept of UAV Recovering System

Jun Jiang, Houde Liu(✉), Bo Yuan, Xueqian Wang, and Bin Liang

Graduate School at Shenzhen, Tsinghua University,
Shenzhen 518055, People's Republic of China
{jiang.jun,liu.hd}@sz.tsinghua.edu.cn

Abstract. This paper introduces a new concept of recovering UAVs to their carrier using manipulator, aiming to better use the carrier's carrying capability. The state-of-the-art of recycling UAVs are stated in the first place, the advantages and the setbacks of the current available recycling systems are introduced, and the reason for the setbacks are further analyzed before this new concept is introduced. To accomplish the basic recovering task, a minimum system configuration that can explain the idea is introduced and the model of the system is built based on several important assumptions. To further explain how the system works, a simulation based on the above configuration is given. The simulation result indicates that the system can fulfill the task of recovering the UAV, and the result also verified the efficiency of the new system, which implies its potential usefulness in the future application.

Keywords: Multi-copter · Manipulator · UAV recovering

1 Introduction

The multi-copter has been a hot topic in scientific research field and also in commercial field for more than a decade. Its indomitable vitality originates from its irreplaceable advantages, which includes but not limited to: agile, light, portable, simple structure, small noise, cheap, foldable, reliable, small vibration, maintenance friendly, and etc. But the disadvantages of this aircraft are also obvious and lethal: short duration, low capacity, unstable, small operation range, which hinder the multi-copter from being applied in more broad and important fields. And among these shortcomings, the short duration and small operation range are the 'Achilles' heels'. A nature way of solving this problem is to combine the multi-copter with a kind of long-range-oriented vehicle to form a new almighty system. And many attempts have been made to build such systems.

A group of researchers focus on developing robust control algorithm for precise landing on the traditional moving platforms. Literature [1] developed a joint decentralized controller for the landing of a quadrotor on skid-steered UGV, the instability problem due to time delay was solved by introducing a RFDE method. Literature [2] designed a control structure by combing estimation module, trajectory module, and tracking module together for fast and precise landing of the quadrotor. The proposed controller proves to be efficient in leading the quadrotor onto the platform. Tang [3] designed a longitudinal-constant-velocity guiding method for docking a quadrotor, the

© Springer Nature Switzerland AG 2019
H. Yu et al. (Eds.): ICIRA 2019, LNAI 11742, pp. 327–338, 2019.
https://doi.org/10.1007/978-3-030-27535-8_30

inner-loop controller is designed to aligns the quadrotor to the carrier's direction, and an augmented estimator is developed for wind rejection. A good amount of work has been done for the navigating the quadrotor to the target. In paper [4], visual servoing method is applied to control the quadrotor towards the moving target, and the variables needed by the controller is reduced to a limited margin. Paper [5] innovatively used a smartphone as the omnidirectional vision acquisition and combined this information with the dynamic model in order to estimate the states of the moving platform. Paper [6] developed non-linear model predictive method to land the quadrotor onto a inclined platform. The proposed system imitates the landing situation on the ship deck. In paper [7], a CPU/GPU based real-time system for relative pose estimation is designed, the system works at a rate of 30 fps, which is sufficient for landing. Paper [8] considered the uncertainties in the land proceeding and used L_1 adaptive loop to enhance the tracking velocity commands. Paper [9] integrated the information of laser and vision to localize the moving platform, and estimate the pose of the deck using a downward facing monocular camera.

The focus of current solution of recovering a quadrotor is to enhance the landing precision of the multi-copter on a deck built for recovering. As the aforementioned literatures covers, the key points of recovering the quadrotor lies in precise localization and the precise position estimation either in absolute or in relative form. The weak points of these methods are: (1), Due to the under-actuated feature, the quadrotor cannot land precisely on the expected point when suffering from constant horizontal disturbance; (2), Traditional precise localization systems are too heavy for the small-sized quadrotors, and low precise sensors are not qualified for precise localization; (3), The decks for recovering quadrotor occupies too much space, and therefore the space utilization is low; (4), The recovered quadrotor cannot be further manipulated after landing onto a deck.

To overcome the weaknesses mentioned above, this paper introduces a new concept of recovering multi-copter system. By replacing the deck with a manipulator, the new system can recover the multi-copter in several more efficient ways. The paper evolves in this way: The following paragraph describes the composition and configuration of the system. Section 3 builds the model of the combined system. A simulation in Sect. 4 was conducted to show the feasibility of the new concept system.

2 System Configuration and Modeling

2.1 System Configuration

The configuration of the system is depicted by Fig. 1. There are four main components in this system: The carrier, the manipulator, the launched aircraft, and the ground station. The carrier in the system usually refers to the aircrafts that are has the complementary characters vs. the launched aircraft. In this paper, the carrier (labeled by 1) is a fixed-wing aircraft, manned or unmanned, and the launched aircraft (labeled by 3) is a multi-copter. The manipulator (labeled by 2) is a 3DOF arm which is able to compensate the residual position error between the fixed-wing aircraft and the multi-copter, leaving the remained 3DOF to be tackled by a specially designed connector,

which is not the focus of this paper. To schedule the tasks and monitoring the whole unmanned system, a ground control station (labeled by 4) is included in the system. During the launch operation, the multi-copter manages to stabilize itself despite the uncertain initial states, which is not this paper's focus. During the recovering procedure, the multi-copter first formats with the fixed-wing aircraft, using onboard localization equipment, mainly the compound GPS-based navigation system. Due to the low precision of the GPS, the capture maneuver is not to be executed, this formation stage is considered to be coarse formation. A further more precise formation has to be done. As they come close to each other, the manipulator and the multi-copter locate each other through vision-base measurement, and the wireless communication devices transmit the states that cannot be observed. When permitted, the capture maneuver is executed.

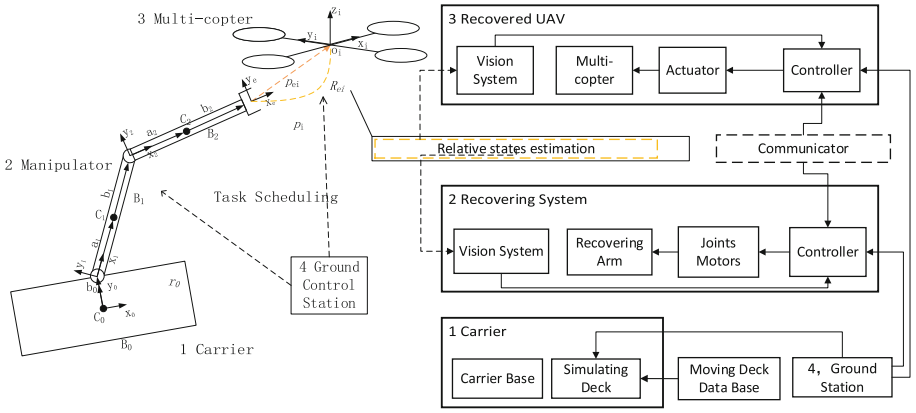

Fig. 1. The concept composes of 4 components: The carrier, the manipulator, the UAV, and the ground control station. The whole system is configured as the right part of the figure shows.

By replacing the deck with a manipulator and space-saving storage device, much space for recovering is saved compared with traditional-landing way. And due to the foldable advantages of the multicopter, much more launched multi-copters are able to be recovered, and therefore, more powerful system is developed. Residue position compensation is the key point of the system and the rest of the paper will focus on explaining it.

2.2 Modeling of the System

To simplify the explanation of the concept, and to make the following modeling and simulation work reasonable, the following assumptions are made:

(1) The manipulator together with its carrier moves at a constant velocity.
(2) All parts of the system are considered as rigid body.
(3) The quadrotor is symmetry, and the joint coincidence with the CoM (Centre of Mass)

(4) The two pats are allowed to get all necessary information from each other.
(5) The carrier is much bigger than the manipulator, so the interaction is neglected.
(6) The weight of the quadrotor is within the capability of the manipulator.
(7) The wind has effect on the quadrotor, but has no effect on the manipulator
(8) The end effector of the manipulator manages to grasp the quadrotor only if the distance between the CoM of the quadrotor and the end effector is smaller than a given value, despite of the other states of the quadrotor.

Figure 2 shows the coordinate frames of the system. Global coordinate frame is set at the bottom of the first link. For link i: m_i stands for the mass, ${}^0\boldsymbol{v}_{\mathrm{iC}}$ stands for the speed of the CoM, l_i stands for its length, $\mathbf{r}_{i\mathrm{COM}}$ stands for the vector from the origin to the CoM, q_i stands for the angle, $\boldsymbol{\omega}_i$ stand for the angle velocity wrt. ith coordinate frame, ${}_0\boldsymbol{\omega}_{i\mathrm{C}}$ stands for the angle velocity wrt. the global coordinate frame, $\boldsymbol{\tau}_i$ stands or the torque exerted on the joint, ${}^{i\mathrm{C}}\mathbf{I}_i = \mathrm{diag}(\mathrm{I}_{i11}, \mathrm{I}_{i22}, \mathrm{I}_{i33})$ is the inertial wrt. ith coordinate frame, ${}^0\boldsymbol{T}_{i\mathrm{S}}$, ${}^{i\mathrm{S}}\boldsymbol{T}_{i\mathrm{C}}$, ${}^{i\mathrm{S}}\boldsymbol{T}_{i\mathrm{E}}$, ${}^{i\mathrm{S}}o_{i\mathrm{C}}$, ${}^{i\mathrm{S}}o_{i\mathrm{E}}$ are the transition matrix where the S, E, C in the subscribes and superscripts are short for 'Start', 'End', and 'CoM'; o_q is the CoM of the Multi-copter, and o_q-$x_qy_qz_q$ is the coordinate attached to it. Both of the two models share the same global coordinate frame, but use different conventions. The manipulator use ENU, and the multi-copter use NED. According to the coordinate frames above, the rotation matrixes of the original coordinates of the links are:

$$ {}^0R_{1S} = \begin{bmatrix} \cos q_1 & -\sin q_1 & 0 \\ \sin q_1 & \cos q_1 & 0 \\ 0 & 0 & 1 \end{bmatrix} = \begin{bmatrix} \mathrm{c}q_1 & -\mathrm{s}q_1 & 0 \\ \mathrm{s}q_1 & \mathrm{c}q_1 & 0 \\ 0 & 0 & 1 \end{bmatrix} \tag{1} $$

$$ {}^1R_{1post} = Rx(90) = \begin{bmatrix} 1 & 0 & 0 \\ 0 & 0 & -1 \\ 0 & 1 & 0 \end{bmatrix} \tag{2} $$

$$ {}^{1post}R_{2S} = Rz(q_2) = \begin{bmatrix} \mathrm{c}q_2 & -\mathrm{s}q_2 & 0 \\ \mathrm{s}q_2 & \mathrm{c}q_2 & 0 \\ 0 & 0 & 1 \end{bmatrix} \tag{3} $$

$$ {}^{2E}R_{3S} = \begin{bmatrix} \mathrm{c}q_3 & -\mathrm{s}q_3 & 0 \\ \mathrm{s}q_3 & \mathrm{c}q_3 & 0 \\ 0 & 0 & 1 \end{bmatrix} \tag{4} $$

Where, the q_i represents the joint angle i, c and s are short for cosine and sine. According to the Lagrange method, the torque exerted on joint i can be computed as,

$$ u_i = \frac{d}{dt}\frac{\partial L}{\partial \dot{\boldsymbol{q}}_i} - \frac{\partial L}{\partial \boldsymbol{q}_i} \tag{5} $$

Where $L = T - U$, and T is the kinetic energy and U is the potential energy of the manipulator. And according to König's theorem,

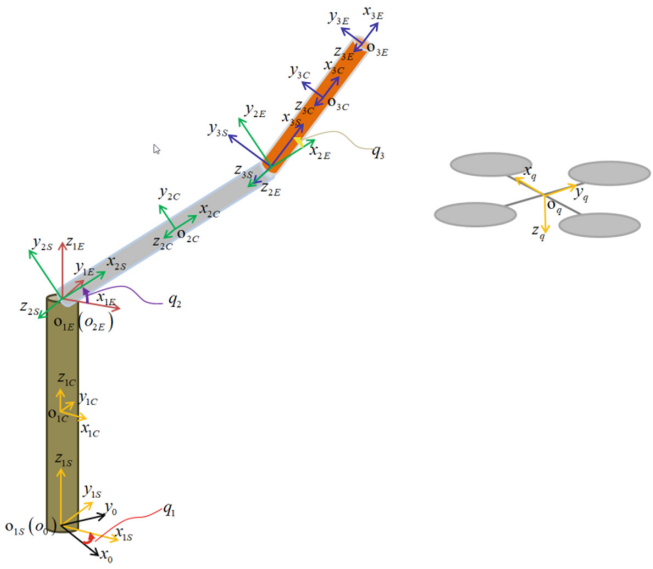

Fig. 2. The coordinate frames of the system.

$$T = \frac{1}{2}\sum m\boldsymbol{v}_{iC}^T\boldsymbol{v}_{iC} + \frac{1}{2}\sum \boldsymbol{\omega}_i^T\boldsymbol{I}_i\boldsymbol{\omega}_i \tag{6}$$

$$U = \sum m_i g h_i \tag{7}$$

Considering the transition relationship between the links depicted by (1)–(4), the model is constructed as the following standard form.

$$\boldsymbol{\tau} = \boldsymbol{M}(\boldsymbol{q})\ddot{\boldsymbol{q}} + \boldsymbol{C}(\boldsymbol{q}, \dot{\boldsymbol{q}}) + \boldsymbol{G}(\boldsymbol{q}) \tag{8}$$

The matrices of $\boldsymbol{M}$, $\boldsymbol{C}$, $\boldsymbol{G}$ are too big to be presented here, please see Appendix 1 for detail. The controlled plant is depicted in the third line in Fig. 3.

For the multi-copter, typical Newton-Euler method is used to develop the model, and to simplify the explanation, the quadrotor is considered as rigid body.

$$\begin{bmatrix} \mathrm{m}_q\boldsymbol{I}_{3\times3} & \boldsymbol{0} \\ \boldsymbol{0} & \boldsymbol{I}_{3\times3} \end{bmatrix} \begin{bmatrix} \dot{\boldsymbol{V}} \\ \dot{\boldsymbol{\omega}}_q \end{bmatrix} + \begin{bmatrix} \dot{\boldsymbol{\omega}}_q \times \mathrm{m}_q\boldsymbol{V} \\ \boldsymbol{\omega}_q \times \mathrm{m}_q\boldsymbol{\omega}_q \end{bmatrix} = \begin{bmatrix} F \\ \boldsymbol{u}_\tau \end{bmatrix} \tag{9}$$

Where, the $\boldsymbol{\omega}_\mathrm{i}$ stand for the angle velocity of the quadrotor, $\mathrm{m_q}$ stands for the weight, the right subtitle is short for quadrotor, $\mathrm{I}_{3\times3}$ is the inertial of the body, V is the linear velocity, F is the total thrust and $\boldsymbol{u}_\tau$ is the inner loop torque. The concise form of the quadrotor dynamic is showed as the following equation, and the detail can be seen in Appendix 1.

$$\dot{\boldsymbol{x}} = \boldsymbol{f}(\boldsymbol{x}, \boldsymbol{u}) \tag{10}$$

Where, $\boldsymbol{x} = \left[\phi\ \theta\ \psi\ \omega_p\ \omega_q\ \omega_r\ x\ y\ z\ \dot{x}\ \dot{y}\ \dot{z}\right]^T$. The items in the vector $\boldsymbol{x}$ are roll angle, pitch angle, yaw angle, roll angle velocity, pitch angle velocity, yaw angle velocity, position in x axis, position in y axis, position in z axis, the rest three are the velocities. $\boldsymbol{u} = \left[F\ \tau_x\ \tau_y\ \tau_z\right]^T$, the items in the vector $\boldsymbol{u}$ are the resultant force, and the torques on the x_q, y_q, z_q body axis.

3 System Control Design

As this paper aims at introducing the new system, simple controllers for each subsystem are designed. Both of the two controllers are supposed to have the full information of each other's, and in this design, the manipulator gets the states of the multicopter and uses it for the planning.

The mission is accomplished when the end point of the manipulator coincide with the CoM of the multi-copter, so our aim is to drive the manipulator to the position of the multi-copter. We first set a rally point for the multi-copter, which is within the manipulator's working space. The manipulator gets the multi-copter's position and velocity, and plans its movement.

For the control of the arm manipulator, a simple PD + gravity compensation algorithm is applied. In Fig. 3, $\boldsymbol{x}_d$ is the state of the multi-copter, and is used for planning. The inverse kinetic of the manipulator is easily got, and can be seen in Appendix 3.

The PD + gravity compensation controller is given in the second line in Fig. 3 and is rewritten as (11), the input of the desired joint angles are from the inverse kinetic of the manipulator, which is based on the multi-copter's current states.

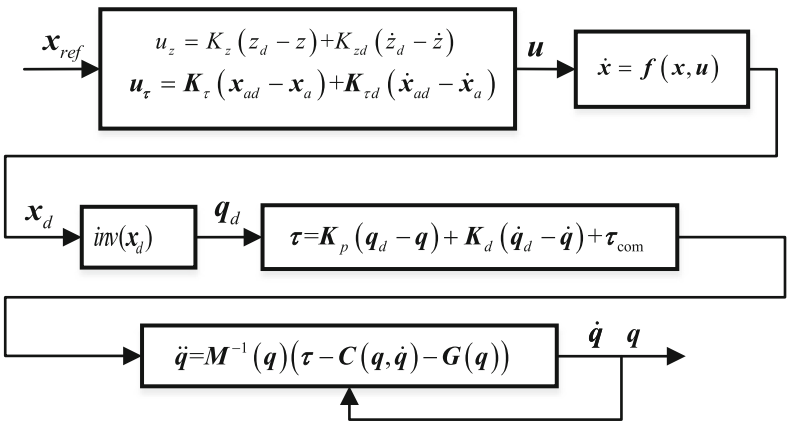

Fig. 3. The control structure of the manipulator.

$$\boldsymbol{\tau} = \boldsymbol{K}_p(\boldsymbol{q}_d - \boldsymbol{q}) + \boldsymbol{K}_d(\boldsymbol{\omega}_d - \boldsymbol{\omega}) + \boldsymbol{\tau}_{com} \tag{11}$$

Where, $\boldsymbol{\tau}_{\mathrm{com}}$ is the gravity compensation torque, and $\boldsymbol{q}_{\mathrm{d}} = [q_{1\mathrm{d}}\ q_{2\mathrm{d}}\ q_{3\mathrm{d}}]^{\mathrm{T}}$ is for the desired angle of the joints. And $\boldsymbol{\omega}_{\mathrm{d}} = [\omega_{1\mathrm{d}}\ \omega_{2\mathrm{d}}\ \omega_{3\mathrm{d}}]^{\mathrm{T}}$ stands for the desired angle velocities of the joints. The gravity compensation item is the function of q_i, l_i, and m_i, and can be easily calculated as (12):

$$\boldsymbol{\tau}_{com} = \begin{bmatrix} 0 \\ \frac{l_3}{2} m_3 g \cos(q_2 + q_3) + \frac{l_2}{2} m_2 g \cos q_2 + m_3 g l_2 \cos q_2 \\ \frac{l_3}{2} m_3 g \cos(q_2 + q_3) \end{bmatrix} \tag{12}$$

For the multi-copter, a cascade structure controller is designed. And for the outer loop control:

$$u_z = K_z(z_d - z) + K_{zd}(\dot{z}_d - \dot{z}) \tag{13a}$$

$$F = m(g - u_z)/\cos\phi\cos\theta \tag{13b}$$

As the multi-copter works at the equilibrium, design two temporary states for horizontal movement as in (14b) and (14c), and are calculated by (14a),

$$\boldsymbol{u}_{xy} = \begin{bmatrix} u_{xd}\ u_{yd} \end{bmatrix}^T = \boldsymbol{K}_{xy}\left(\boldsymbol{x}_{xyd} - \boldsymbol{x}_{xy}\right) + \boldsymbol{K}_{xyd}\left(\dot{\boldsymbol{x}}_{xyd} - \dot{\boldsymbol{x}}_{xy}\right) \tag{14a}$$

$$u_{xd} = \cos\phi\sin\theta\cos\psi + \sin\phi\sin\psi \tag{14b}$$

$$u_{yd} = \cos\phi\sin\theta\sin\psi - \sin\phi\cos\psi \tag{14c}$$

The desired angles are given as (15a) and (15b), and the inner loop control algorithm is given as (15c), the desired yaw is constantly zero and not to be shown here:

$$\phi_d = a\sin\left(\sin\psi u_{xd} - \cos\psi u_{yd}\right) \tag{15a}$$

$$\theta_d = a\sin\left(\left(\cos\psi u_{xd} + \sin\psi u_{yd}\right)/\cos\phi_d\right) \tag{15b}$$

$$\boldsymbol{u}_\tau = \boldsymbol{K}_\tau(\boldsymbol{x}_{ad} - \boldsymbol{x}_a) + \boldsymbol{K}_{\tau d}(\dot{\boldsymbol{x}}_{ad} - \dot{\boldsymbol{x}}_a) \tag{15c}$$

4 Recovering Simulation

4.1 Simulation Condition Set

The initial states of the angles of the manipulator are: $[0\ 0\ 0]^{\mathrm{T}}$. The desired tip position of the manipulator keeps with the CoM of the quadrotor in real time.

For the manipulator, a PD + gravity compensation controller is designed.

Link1: cylinder: radius: 0.03 m, length: 0.5 m, density: 2700 kg/m^3.
Link2: cuboid: 0.05*0.05*0.5 m density: 2700 kg/m^3.
Link3: cuboid: 0.05 * 0.05 * 0.5 m density: 2700 kg/m^3.

$$K_{arm}=\begin{bmatrix} 20 & 6 & 0 & 0 & 0 & 0 \\ 0 & 0 & 40 & 15 & 0 & 0 \\ 0 & 0 & 0 & 0 & 20 & 6 \end{bmatrix}$$

The parameters of the quadrotor are: m = 1.64, l = 0.4 m; I_{xx} = 0.044 kg m^2, I_{yy} = 0.044 kg m^2, I_{zz} = 0.088 kg m^2, J_r = 90*10^{-6}; For the simulation, the initial states of the quadrotor is set to be a little off its equilibrium, which are, angle: [0.5 0.5 0]^T, angle velocity: [0 0 0]^T, position: [2.657 2 3]^T, velocity: [0 0 0]^T. The desired position: [0.5 0.5 0.5]^T, and the desired velocity: [0 0 0]^T. In this scenario, the yaw angle is insignificant, and is constantly set to zero (Fig. 4).

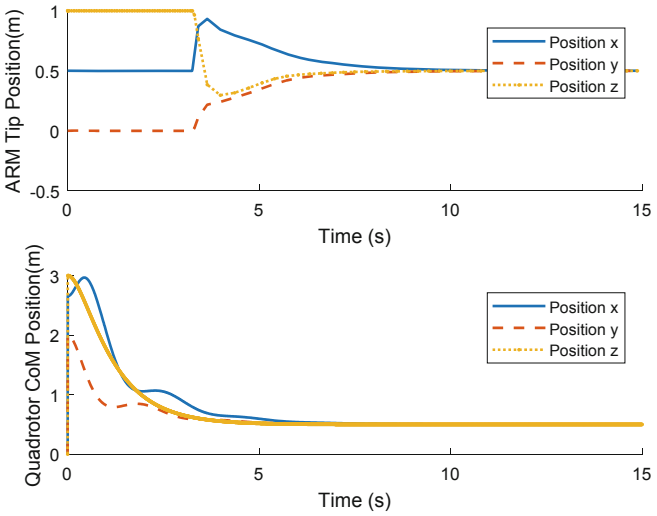

Fig. 4. The positions vs. time of the system components.

The control matrixes are as follows:

$$K_z = [3.1623 \;\; 4.0404]$$

$$K_{xy}=\begin{bmatrix} 0.25 & 0.4195 & 0 & 0 \\ 0 & 0 & 0.25 & 0.4195 \end{bmatrix}$$

$$K_\tau = \begin{bmatrix} 12.2474 & 4.5911 & 0 & 0 & 0 & 0 \\ 0 & 0 & 12.2474 & 4.5911 & 0 & 0 \\ 0 & 0 & 0 & 0 & 37.4166 & 14.3731 \end{bmatrix}$$

The quadrotor enters the manipulator's scope at about 3rd second, and triggers the actuation of the manipulator, then the quadrotor settles at about 8th second. And the manipulator carries on pursuing the CoM of the quadrotor, and the tip of it finally reaches the CoM of the quadrotor at about 10th second (Fig. 5).

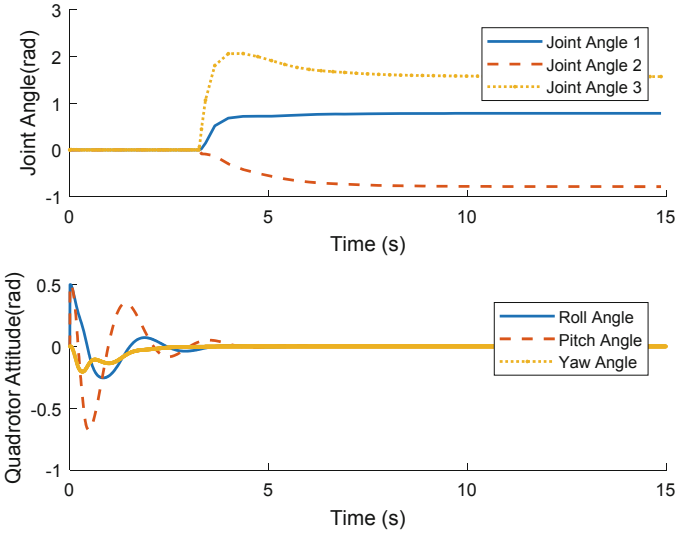

Fig. 5. Angles in the system.

This figure shows the angles vs. time of the quadrotor and the manipulator. The quadrotor settles at about 5th second. As the manipulator has a limited scope, the joints start at about 3rd second when the quadrotor enters its scope, and as the tip of the manipulator reaches the multi-copter's CoM, the joints' angles of the manipulator converge.

5 Conclusion

A new concept of recovering a UAV to its carrier is proposed, and the system is explained by illustrating the composition of the system and the operating mechanism. To give an intuitive impression of the system, the model of the system is built and a simulation was conducted. The result shows that, the system is able to recover the UAV, and the combination of the system implies its potential practicality. The proposed concept can be further used in more dynamic scenarios, such as air-based systems, and become more useful in more application fields.

Acknowledgments. This work was partially supported by the National Natural Science Foundation of China (No. U1813216 and No. 61803221), the Science and Technology Research Foundation of Shenzhen (JCYJ20160301100921349 and JCYJ20170817152701660).

Appendix 1

$$\begin{pmatrix} \dot{x}_1 \\ \dot{x}_2 \\ \dot{x}_3 \\ \dot{x}_4 \\ \dot{x}_5 \\ \dot{x}_6 \\ \dot{x}_7 \\ \dot{x}_8 \\ \dot{x}_9 \\ \dot{x}_{10} \\ \dot{x}_{11} \\ \dot{x}_{12} \end{pmatrix} = \begin{pmatrix} x_4 + x_5 \sin x_1 \tan x_2 + x_6 \cos x_1 \tan x_2 \\ x_5 \cos x_1 - x_6 \sin x_1 \\ (x_5 \sin x_1 + x_6 \cos x_1)/\cos x_2 \\ \big((I_{yy} - I_{zz})x_5 x_6 - x_5 \Omega Jr\big)/I_{xx} \\ ((I_{zz} - I_{xx})x_4 x_6 + x_4 \Omega Jr)/I_{yy} \\ \big((I_{xx} - I_{yy})x_4 x_5 - \dot{\Omega} Jr\big)/I_{zz} \\ x_{10} \\ x_{11} \\ x_{12} \\ 0 \\ 0 \\ g \end{pmatrix} + \begin{pmatrix} 0 & 0 & 0 & 0 \\ 0 & 0 & 0 & 0 \\ 0 & 0 & 0 & 0 \\ 0 & 1/I_{xx} & 0 & 0 \\ 0 & 0 & 1/I_{yy} & 0 \\ 0 & 0 & 0 & 1/I_{zz} \\ 0 & 0 & 0 & 0 \\ 0 & 0 & 0 & 0 \\ 0 & 0 & 0 & 0 \\ \frac{\cos x_1 \sin x_2 \cos x_3 + \sin x_1 \sin x_3}{m} & 0 & 0 & 0 \\ \frac{\cos x_1 \sin x_2 \sin x_3 - \sin x_1 \cos x_3}{m} & 0 & 0 & 0 \\ -\frac{\cos x_1 \cos x_2}{m} & 0 & 0 & 0 \end{pmatrix} \begin{pmatrix} F \\ \tau_{1q} \\ \tau_{2q} \\ \tau_{3q} \end{pmatrix}$$

Appendix 2

$$\boldsymbol{M} = \begin{bmatrix} m_{11} & m_{12} & m_{13} \\ m_{21} & m_{22} & m_{23} \\ m_{31} & m_{32} & m_{33} \end{bmatrix}$$

$$\begin{aligned} m_{11} &= \frac{\mathrm{I}_{2xx} + \mathrm{I}_{3xx} + \mathrm{I}_{2yy}}{2} + \mathrm{I}_{3yy} + \mathrm{I}_{1zz} - \frac{\big(\mathrm{I}_{3xx} + \mathrm{I}_{3yy} + \mathrm{m}_3\mathrm{r}_{3com}^2\big)\cos(2q_2 + 2q_3)}{2} \\ &\quad + \frac{\mathrm{l}_2^2\mathrm{m}_3 + \mathrm{m}_2\mathrm{r}_{2com}^2 + \mathrm{m}_3\mathrm{r}_{3com}^2}{2} + \frac{\big(\mathrm{I}_{2yy} - \mathrm{I}_{2xx} + \mathrm{l}_2^2\mathrm{m}_3 + \mathrm{m}_2\mathrm{r}_{2com}^2\big)\cos 2q_2}{2} \\ &\quad + \mathrm{l}_2\mathrm{m}_3\mathrm{r}_{3com}\cos q_3 + \mathrm{l}_2\mathrm{m}_3\mathrm{r}_{3com}\cos(2q_2 + q_3) \\ m_{12} &= 0 \\ m_{13} &= 0 \\ m_{22} &= \mathrm{m}_3\mathrm{l}_2^2 + 2\mathrm{m}_3\cos q_3\mathrm{l}_2\mathrm{r}_{3com} + \mathrm{m}_2\mathrm{r}_{2com}^2 + \mathrm{m}_3\mathrm{r}_{3com}^2 + \mathrm{I}_{2zz} + \mathrm{I}_{3zz} \\ m_{23} &= m_{32} = \mathrm{m}_3\mathrm{r}_{3com}^2 + \mathrm{l}_2\mathrm{m}_3\cos q_3\mathrm{r}_{3com} + \mathrm{I}_{3zz} \\ m_{33} &= \mathrm{m}_3\mathrm{r}_{3com}^2 + \mathrm{I}_{3zz} \end{aligned}$$

$$\boldsymbol{C}(\boldsymbol{q},\dot{\boldsymbol{q}}) =$$

$$\begin{bmatrix}
-\dot{q}_1\left(\left(\mathrm{I}_{2yy}\dot{q}_2 - \mathrm{I}_{2xx}\dot{q}_2 + \mathrm{l}_2^2\mathrm{m}_3\dot{q}_2 + \mathrm{m}_2\dot{q}_2 r_{2com}^2\right)\sin 2q_2\right. \\
+\left(\mathrm{I}_{3yy}\dot{q}_3 + \mathrm{I}_{3yy}\dot{q}_2 - \mathrm{I}_{3xx}\dot{q}_3 - \mathrm{I}_{3xx}\dot{q}_2 + \mathrm{m}_3\dot{q}_2 r_{3com}^2 + \mathrm{m}_3\dot{q}_3 r_{3com}^2\right)\sin(2q_2+2q_3) \\
+(2\mathrm{l}_2\mathrm{m}_3\dot{q}_2 r_{3com} + \mathrm{l}_2\mathrm{m}_3\dot{q}_2 r_{3com})\sin(2q_2+q_3) + \mathrm{l}_2\mathrm{m}_3\dot{q}_3 r_{3com}\sin q_3) \\
\left(\left(\mathrm{I}_{2yy}\dot{q}_1^2 - \mathrm{I}_{2xx}\dot{q}_1^2\right)\sin 2q_2\right)/2 - \left(\left(\mathrm{I}_{3xx}\dot{q}_1^2 + \mathrm{I}_{3yy}\dot{q}_1^2\right)\sin(2q_2+2q_3)\right)/2 \\
+\left(\left(\mathrm{l}_2^2\mathrm{m}_3\dot{q}_1^2 + \mathrm{m}_2\dot{q}_1^2 r_{2com}^2\right)\sin 2q_2\right)/2 + (\mathrm{m}_3\dot{q}_1^2 r_{3com}^2\sin(2q_2+2q_3))/2 \\
-\mathrm{l}_2\mathrm{m}_3\dot{q}_3^2 r_{3com}\sin q_3 + \mathrm{l}_2\mathrm{m}_3\dot{q}_1^2 r_{3com}\sin(2q_2+q_3) - 2\mathrm{l}_2\mathrm{m}_3\dot{q}_2\dot{q}_3 r_{3com}\sin q_3 \\
(\mathrm{I}_{3yy}\dot{q}_1^2\sin(2q_2+2q_3))/2 - (\mathrm{I}_{3xx}\dot{q}_1^2\sin(2q_2+2q_3))/2 \\
+(\mathrm{m}_3\dot{q}_1^2 r_{3com}^2\sin(2q_2+2q_3))/2 + (\mathrm{l}_2\mathrm{m}_3\dot{q}_1^2 r_{3com}\sin q_3)/2 \\
+\mathrm{l}_2\mathrm{m}_3\dot{q}_2^2 r_{3com}\sin q_3 + (\mathrm{l}_2\mathrm{m}_3\dot{q}_1^2 r_{3com}\sin(2q_2+q_3))/2
\end{bmatrix}$$

$$\boldsymbol{G}(\boldsymbol{q}) =$$

$$\begin{bmatrix}
0 \\
-\mathrm{m}_3\mathrm{g}(r_{3com}(\cos q_2\cos q_3 - \sin q_2\sin q_3) + \mathrm{l}_2\cos q_2) - \mathrm{m}_2\mathrm{g}r_{2com}\cos q_2 \\
-\mathrm{m}_3\mathrm{g}r_{3com}(\cos q_2\cos q_3 - \sin q_2\sin q_3)
\end{bmatrix}$$

Appendix 3

$$q_1 = a\tan 2\left(x_y, x_x\right)$$

$$q_3 = \pm\left(\pi - a\cos\left(\frac{(x_z - l_1)^2 + x_x^2 + x_y^2 - l_2^2 - l_3^2}{2l_2 l_3}\right)\right)$$

$$q_2 = a\tan 2\left(x_z - l_1, \sqrt{x_x^2 + x_y^2}\right) - a\tan 2(l_2 + l_3\cos q_3, l_3\sin q_3)$$

References

1. Daly, J.M., Yan, M., Waslander, S.L.: Coordinated landing of a quadrotor on a skid-steered ground vehicle in the presence of time delays. Auton. Robots **38**(2), 179–191 (2015)
2. Botao, H., Lu, L., Mishra, S.: Fast, safe and precise landing of a quadrotor on an oscillating platform. In: 2015 American Control Conference (ACC), pp. 3836–3841 (2015)
3. Tang, Z., et al.: Homing on a moving dock for a quadrotor vehicle. In: 2015 IEEE Region 10 Conference, TENCON 2015, pp. 1–6 (2015)
4. Zheng, D., Wang, H., Chen, W.: Image-based visual tracking of a moving target for a quadrotor. In: 2017 11th Asian Control Conference (ASCC), pp. 198–203 (2017)

5. Kim, J., et al.: Outdoor autonomous landing on a moving platform for quadrotors using an omnidirectional camera. In: 2014 International Conference on Unmanned Aircraft Systems (ICUAS), pp. 1243–1252 (2014)
6. Vlantis, P., et al.: Quadrotor landing on an inclined platform of a moving ground vehicle. In: 2015 IEEE International Conference on Robotics and Automation (ICRA), pp. 2202–2207 (2015)
7. Benini, A., Rutherford, M.J., Valavanis, K.P.: Experimental evaluation of a real-time GPU-based pose estimation system for autonomous landing of rotary wings UAVs. Control Theory Technol. **16**(2), 145–159 (2018)
8. Jung, Y., Cho, S., Shim, D.H.: A trajectory-tracking controller design using L1 adaptive control for multi-rotor UAVs. In: 2015 International Conference on Unmanned Aircraft Systems (ICUAS), pp. 132–138 (2015)
9. Chen, X., et al.: System integration of a vision-guided UAV for autonomous landing on moving platform. In: IEEE International Conference on Control and Automation, pp. 761–766 (2016)